

Article

Blue Emitting Star-Shaped and Octasilsesquioxane-Based Polyanions Bearing Boron Clusters. Photophysical and Thermal Properties [†]

Justo Cabrera-González, Mahdi Chaari , Francesc Teixidor, Clara Viñas  and Rosario Núñez ^{*} 

Institut de Ciència de Materials de Barcelona (ICMAB-CSIC), Campus U.A.B., 08193 Bellaterra, Barcelona, Spain; justocab@ucm.es (J.C.-G.); ch.mahdi39@gmail.com (M.C.); teixidor@icmab.es (F.T.); clara@icmab.es (C.V.)

^{*} Correspondence: rosario@icmab.es; Tel.: +34-93-580-1853

[†] Dedicated to Professor Bohumil Štibr (1940-2020), who unfortunately passed away before he could reach the age of 80, in the recognition of his outstanding contributions to boron chemistry. F.T. and C.V. express their sincere condolences on the loss of a great friend.

Academic Editors: Igor B. Sivaev, Narayan S. Hosmane and Bohumír Grüner

Received: 19 February 2020; Accepted: 5 March 2020; Published: 7 March 2020



Abstract: High boron content systems were prepared by the peripheral functionalisation of 1,3,5-triphenylbenzene (TPB) and octavinylsilsesquioxane (OVS) with two different anionic boron clusters: *closo*-dodecaborate (B₁₂) and cobaltabisdicarbollide (COSAN). TPB was successfully decorated with three cluster units by an oxonium ring-opening reaction, while OVS was bonded to eight clusters by catalysed metathesis cross-coupling. The resulting compounds were spectroscopically characterised, and their solution-state photophysical properties analysed. For TPB, the presence of COSAN dramatically quenches the fluorescence emission ($\lambda_{em} = 369$ nm; $\Phi_F = 0.8\%$), while B₁₂-substituted TPB shows an appreciable emission efficiency ($\lambda_{em} = 394$ nm; $\Phi_F = 12.8\%$). For octasilsesquioxanes, the presence of either COSAN or B₁₂ seems to be responsible for ~80 nm bathochromic shift with respect to the core emission, but both cases show low emission fluorescence ($\Phi_F = 1.4$ – 1.8%). In addition, a remarkable improvement of the thermal stability of OVS was observed after its functionalisation with these boron clusters.

Keywords: boron clusters; boranes; metallocarboranes; triphenylbenzene; octasilsesquioxanes; luminescence

1. Introduction

Over the last ten years, a great effort from the scientific community has been done to develop luminescent boron cluster-based materials. The direct or indirect binding of icosahedral boron clusters to luminophores cause a significant effect on the photoluminescent behaviour of the final materials [1,2]. Polyhedral boranes are characterised by their three-dimensional (3D) structure with electrons' delocalisation inside the cage [3,4]. Among the boron cluster families, the most extensively studied are those of the carborane class. They have a highly polarisable σ -aromatic character and interact electronically with π -conjugated systems [5,6]. The interest in carboranes and metallocarboranes as potential units for molecular materials might be endorsed to their remarkable chemical, thermal, and biological stabilities [7–17]. Owing to the properties above of carboranes, they have been used as exceptional building blocks for developing a large variety of fluorescent carborane-containing molecules, in which the cluster is usually linked to a fluorescent π -conjugated organic system, either directly by the C_c [18–30] or through one spacer [7–9,31–39].

In addition to the properties described for carboranes, the presence of a cobalt metal centre in the cobaltabisdicarbollide anion (COSAN, [3,3'-Co(C₂B₉H₁₁)₂]⁻) confers to these cluster unique

redox properties, that can be tuned upon dehydrohalogenation [40–42], as well as extraordinary high chemical and thermal stability [43–45]. This anion has a high molecular volume, low nucleophilic character, and low charge density because the negative charge is distributed between 45 atoms [46]. The protonated form and sodium salt of COSAN cluster have shown exceptional physicochemical properties such as amphiphilicity, leading to supramolecular interactions and self-assembling in water [47–53]. All these properties and the biocompatibility of COSAN make this cluster a promising scaffold for biomedical applications [13,54–60].

From the wide variety of boron clusters, the dodecahydro-*closo*-dodecaborate dianion [61], commonly referred to as *closo*-dodecaborate (*closo*-B₁₂, [B₁₂H₁₂]²⁻), has received increased attention due to its high chemical, thermal, and hydrolytic stability [62,63], as well as good aqueous solubilising agent [44,64]. Moreover, the water solubility of sodium form of *closo*-B₁₂ added to its low toxicity [65], makes this anion and its derivatives ideal candidates to design pharmacophores [66–69]. Additionally, [B₁₂H₁₂]²⁻ has found applications in material sciences as molecular motors and actuators in nanodevices [70] or energy storage through the design of stable and rechargeable batteries [71].

On the other hand, 1,3,5-triphenylbenzene (TPB) is a thermally and photochemically stable fluorophore with π electron-rich properties [72]. With different substitutions at the peripheral phenyl rings, TPB has emerged as one of the most useful building blocks for a wide variety of organic light emitting materials [73]. Previously, our group and others have reported different sets of star-shaped molecules where the TPB acts as the core of carboranyl-functionalised dendrimers that exhibit fluorescence properties [9,74,75]. Moreover, polyanionic Fréchet-type poly(aryl-ether) dendrimers grown from the TPB core were decorated with three, six, or twelve terminal COSAN units; nevertheless contrary to the above carboranyl-containing poly(aryl-ether) dendrimers functionalised with *o*-carborane clusters, these do not show luminescence properties, as a quenching of the fluorescence takes place after functionalisation with COSAN derivatives [76].

Another outstanding family of compounds used as scaffolds are the octasilsesquioxane cubes (T₈), with general formula [RSiO_{1.5}]₈. Their 3D structure, chemical versatility in functionality, high robustness and thermal stability, as well as their mechanical, electronic or optical properties [77–79], make silsesquioxane-based materials very useful in a wide range of applications: Thermally and chemically resistant polymers and ceramics [80–82], catalysis [83], nanomedicine [84], or optoelectronic materials [85–87], etc. Previously, our group has reported hybrid materials based on octasilsesquioxane structures decorated with terminal *o*-carborane clusters throughout an organic π -conjugated group that exhibit photoluminescence properties (PL) [8]. These systems were synthesised via olefin cross-metathesis reaction [88–90], between the octavinylsilsesquioxane (OVS) and several *o*-carboranyl-styrene derivatives bearing different substituents at the adjacent C_c atom [8], or by Heck coupling reaction between octa(*p*-bromostyrenyl)silsesquioxane (*p*-BrStyrenylIOS) [88] and carboranyl-styrene derivatives [35] in the presence of a palladium catalyst [7]. In general, all these hybrids exhibit moderate to high fluorescent quantum yields in solution; being the most efficient one that contains the nonsubstituted *o*-carborane unit. We concluded that the final PL properties might be tailored by changing the substituents bound to the C_{cluster}, but also the type of carborane isomer. In these hybrids the POSS cage acts as an organising scaffold, causing restriction of the intramolecular movement of the arms, and avoiding additional intramolecular interactions that could cause the fluorescence quenching in the solution. The aforementioned silsesquioxanes-boron cluster hybrids, and another example of carboranyl substituted octasilsesquioxane [91] have shown remarkable thermal stability. We recently reported the first example of octasilsesquioxane cubes bearing COSAN and FESAN clusters [43], however, there are no examples in the literature of octasilsesquioxane structures functionalised with [B₁₂H₁₂]²⁻. In addition, to the best of our knowledge, the photoluminescence properties of these polyanionic boron rich systems have never been evaluated before.

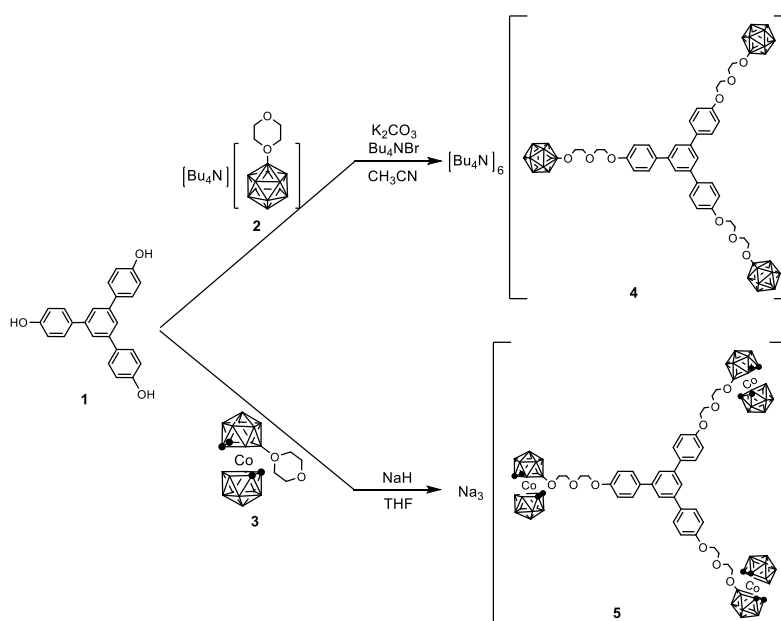
Herein, we report the synthesis, characterisation, and photophysical properties in solution of two polyanionic star-shaped molecules obtained using 1,3,5-triphenylbenzene (TPB) as a core, which is periphery functionalised with three *closo*-B₁₂ or COSAN units. Moreover, a new T₈-based hybrid

decorated with eight *closo*-B₁₂ moieties has also been prepared. Furthermore, thermal and photophysical properties of the latter have been compared to its homologous with COSAN (T₈-COSAN), as previously reported [43].

2. Results and Discussion

2.1. Synthesis and Characterisation

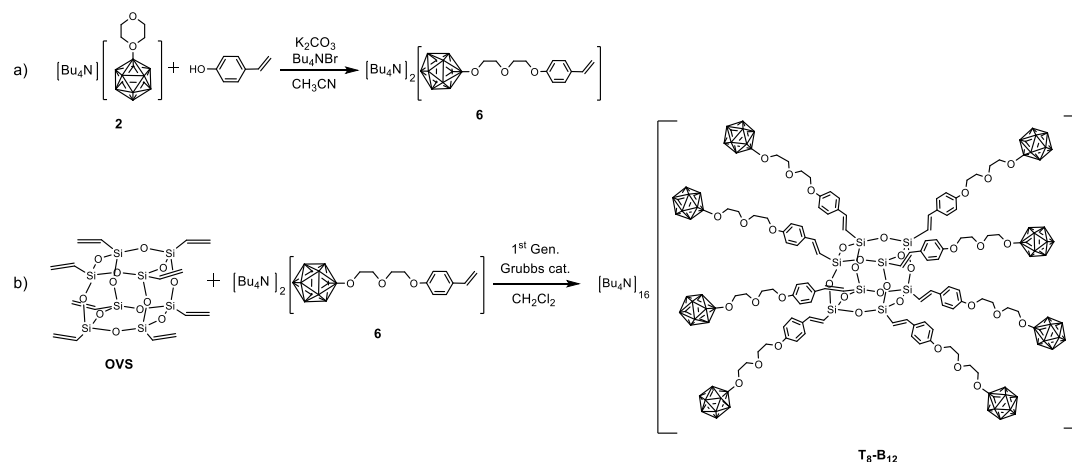
Decoration of the star-shaped core 1,3,5-Tris(4-hydroxyphenyl)benzene (**1**) with the anionic boron clusters was performed via nucleophilic ring-opening reaction of their oxonium-derivatives [92], i.e., [Bu₄N][B₁₂H₁₁(C₄H₈O₂)] (**2**) and [3,3'-Co(8-C₄H₈O₂-1,2-C₂B₉H₁₀)(1',2'-C₂B₉H₁₁)] (**3**) [93,94]. Compound **4** was prepared following previously described conditions [95–100]: Firstly, deprotonation of hydroxy groups in **1** with K₂CO₃ takes place, and secondly, phenoxy moieties undergo a nucleophilic attack promoting the ring-opening reaction of **2**. In a similar manner, compound **5** was synthesised from **1** and COSAN derivative **3** using NaH as a deprotonating agent. In this instance, **5** was obtained as the sodium salt, but Hosmane et al. also have prepared the potassium salt [97]. The reactions were monitored by ¹¹B-NMR spectroscopy by comparison with their parent species, and compounds **4** and **5** were isolated in 57% and 63% yield, respectively (Scheme 1). We previously reported the preparation of metallodendrimers based on the same aromatic core **1** functionalised from **3** to 12 COSAN units through hydrosilylation reactions [76], however, the synthetic pathway described here can be considered a simpler and more efficient approach.



Scheme 1. Synthesis of compounds **4** and **5**.

On the other hand, functionalisation of the octavinylsilsesquioxane (OVS) cube with eight *closo*-dodecaborate units was performed via cross-metathesis reaction, as was previously described for COSAN and FESAN derivatives by our group [43]. Based on that strategy, a new *closo*-dodecaborate precursor bearing a terminal styrene group was prepared by ring-opening reaction of **2** with 4-vinylphenol (Scheme 2a). The evolution of the reaction was also monitored by ¹¹B NMR spectroscopy, and compound **6** was obtained in 72% yield. A successful cross-metathesis reaction of OVS and **6** was achieved using the first generation Grubbs catalyst [101] in CH₂Cl₂ at reflux for 60 h, and around 20% of the excess of **6** was added to ensure the complete functionalisation of the central cube. The cross-metathesis reaction was monitored by ¹H NMR upon the disappearance of the vinyl proton resonances from the Si-CH=CH₂ of OVS (Figure 1). The regio- and stereoselective *E*-isomers of T₈-B₁₂

was obtained in 18% yield (Scheme 2b). It should be noted that the terminal styrene group in **6** confers to this compound a high chemical versatility to use it as starting material in a variety of reactions.



Scheme 2. Synthesis of compounds (a) **6** and (b) **T₈-B₁₂**.

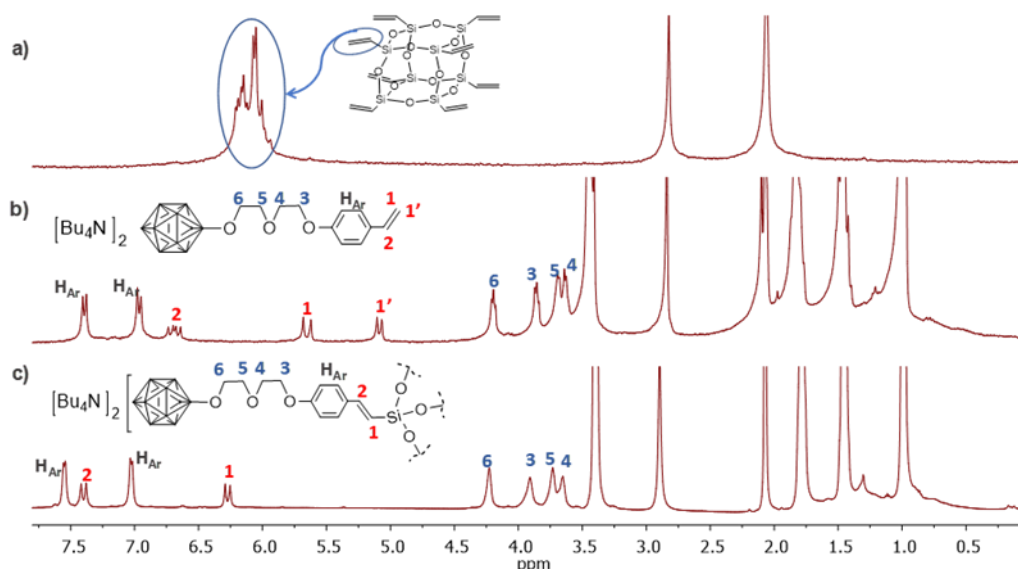


Figure 1. ^1H -NMR spectra in acetone- d_6 of (a) octavinylsilsesquioxane (OVS), (b) compound **6** and (c) **T₈-B₁₂**.

The molecular structures of all the compounds were established using standard spectroscopy techniques: IR-ATR, NMR (^1H , $^{13}\text{C}\{^1\text{H}\}$, and $^{11}\text{B}\{^1\text{H}\}$) (Figure S2–S17), and elemental analysis.

The IR-ATR spectra for those compounds bearing the *closo*-dodecaborate cluster show the typical $\nu(\text{B-H})$ strong bands below 2500 cm^{-1} (**4**, **6**, and **T₈-B₁₂**), while compound **5** exhibit this band around 2534 cm^{-1} . For **T₈-B₁₂**, the characteristic broadband around 1090 cm^{-1} due to the vibration frequency of the Si-O bond is also evident (Figure S17). The ^1H NMR spectra of all compounds show the aromatic resonances corresponding to the phenyl moieties in the region from δ 6.97 to 7.80 ppm, and the $-\text{CH}_2\text{O}-$ groups are identified in their usual range δ 3.43–4.24 ppm. Additionally, COSAN derivative **5** displays two resonances at 4.29 and 4.32 ppm undoubtedly attributed to the $\text{C}_c\text{-H}$ protons, while for **6** appears the characteristic vinylic ($\text{CH}=\text{CH}_2$) distribution as two doublets and one doublet of doublets in the range 5.08–6.69 ppm (Figure 1b). In contrast to **6**, in the ^1H NMR of **T₈-B₁₂** the vinylic signals have disappeared after the cross-metathesis reaction, giving rise to the new vinylene ($\text{CH}=\text{CH}$) resonances as two doublets with an 18 Hz *trans* coupling constant at 6.26 and 7.39 ppm (Figure 1c). The $^{11}\text{B}\{^1\text{H}\}$ NMR

spectrum of **5** shows the typical 1:1:1:1:2:3:3:2:2:1:1 pattern from δ +25 to -28 ppm [95,96,102], and the lowest field resonance is assigned to the [B(8)-O]. For those compounds bearing the *closo*-dodecaborate cluster (**4**, **6**, and **T₈-B₁₂**), the $^{11}\text{B}\{^1\text{H}\}$ NMR spectra show a simpler distribution pattern with a ratio of 1:5:5:1, from +8 to -21 ppm, assigning again the lowest field resonance to the [B(1)-O] [98]. The $^{13}\text{C}\{^1\text{H}\}$ NMR spectra also established the structure of compounds, showing the resonances of aromatic and vinylic carbons for all of them in the region δ 110–160 ppm. Moreover, the terminal vinylic $\text{CH}=\text{CH}_2$ signal at 110.6 ppm displayed for **6** has disappeared after the coupling reaction with OVS, which further confirms the successful synthesis of **T₈-B₁₂**. The $^{13}\text{C}\{^1\text{H}\}$ NMR spectra of the aliphatic ether moieties are shown from δ 67 to 74 ppm, and for compound **5** two additional resonances displayed at 55.2 and 47.2 ppm are attributed to the C_c from COSAN.

2.2. Photophysical Properties

The solution-state photophysical behaviour of compounds, **4–6**, **T₈-B₁₂**, as well as **T₈-COSAN** (Figure S1, previously synthesised by us [43]), were studied by UV–Vis and fluorescence (PL) spectroscopy. Results of the optical properties are shown in Figure 2 and listed in Table 1.

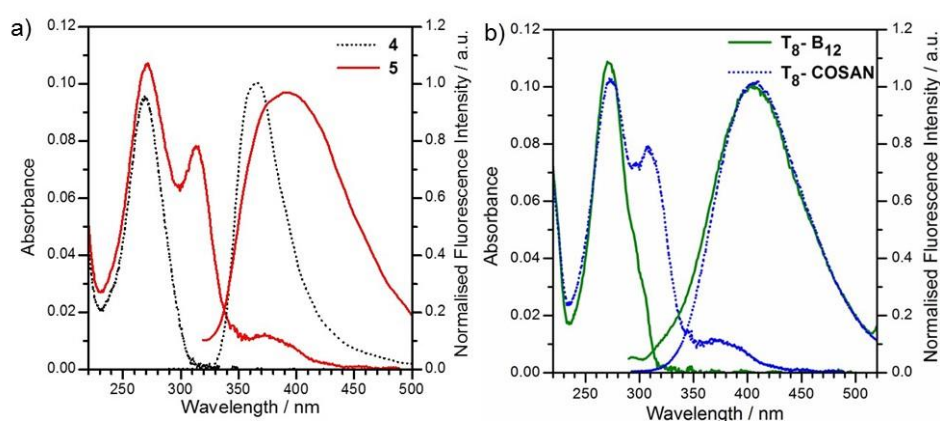


Figure 2. Absorption and emission spectra of (a) **4–5** and (b) **T₈-B₁₂** and **T₈-COSAN** recorded in CH_3CN (au: Arbitrary units).

Table 1. Solution-state photophysical data.

Compounds	$\lambda_{\text{abs}}/\text{nm}$	$\epsilon/\text{M}^{-1}\text{cm}^{-1}$	$\lambda_{\text{em}} (\lambda_{\text{exc}})/\text{nm}$	$\phi_{\text{F}}^{\text{a}}$	Stokes Shift (nm)
4	269	68000	369 (269)	0.128	100
5	272	83000	394 (272)	0.008	122
T₈-B₁₂	270	186000	405 (270)	0.014	136
T₈-COSAN	272	233000	406 (272)	0.018	138

^a Reference compound quinine sulfate (0.5 M H_2SO_4 , $\phi_{\text{F}} = 0.54$).

Inspecting the absorption spectra of **4** and **5** in CH_3CN (Figure 2a), high energy bands found around 270 nm are attributed mainly to the π – π^* transitions occurring within the aromatic core, which are redshifted compared to the maximum at 254 nm reported for TPB [103,104]. This 270 nm band is the main absorption observed for **4**, but additional bands are identified for COSAN derivative **5**: A band at 313 nm and another near 370 nm, which are endorsed to the metallacarborane unit substituted with the $\text{O}-(\text{CH}_2)_2-\text{O}-(\text{CH}_2)_2-$ moiety [105]. Additionally, a weak band around 450–460 nm due to the d–d transition in Co^{III} is also observed [106]. Molar extinction coefficients (ϵ) were determined at their higher absorptions, giving a value of $6.8 \times 10^4 \text{ M}^{-1}\cdot\text{cm}^{-1}$ for **4**, which increases up to $8.3 \times 10^4 \text{ M}^{-1}\cdot\text{cm}^{-1}$ for compound **5**, probably due to some contribution of COSAN cluster at that wavelength range [106]. These ϵ values are also in the range of TPB substituted by hydrosilylation with three COSAN units ($\epsilon = 8.6 \cdot 10^4 \text{ M}^{-1}\cdot\text{cm}^{-1}$) [76]. Regarding the emission properties, both compounds exhibit a single

broadband when excited at their maxima absorption, but a different fluorescence (PL) behaviour is pointed out. In this regard, a remarkable higher PL emission intensity of compound **4**, with a quantum yield value of $\Phi_F = 12.8\%$ is observed, while COSAN derivative **5** do not show appreciable emission, $\Phi_F = 0.8\%$. The low intensity of emission of compound **5** has been ascribed to a quenching process when the COSAN cluster is chemically bonded to the fluorescent core, which has been previously observed for other COSAN-containing fluorophores [1,76]. Nevertheless, when TPB was substituted with *closo*-carborane units through a $-\text{CH}_2-$ spacer, their Φ_F could be modulated from 26% to 55% depending on the substituents at the second C_c [9]. In that case, the presence of *closo*-carborane clusters increased the emission efficiency compared to that reported for pristine TPB ($\Phi_F = 10\%$ in CH_2Cl_2) [75]. These results confirm that the inherent nature of COSAN induces a notable PL quenching of TPB, while this is not occurring for compound **4** substituted with *closo*-dodecaborate cluster. It should be noted that comparable behaviour was observed when **2** and **3** were appended to organotin fluorophores: While the presence of COSAN reduced the emission efficiency to $\Phi_F \leq 7\%$, the substitution of the tin complexes with one *closo*-dodecaborate unit increased this value up to $\Phi_F = 49\%$ [96]. In addition to the different PL emission efficiency of **4** and **5**, the former exhibits a maximum emission (λ_{em}) centred at 364 nm, that is in the region of carboranes-bearing TPB [9], but blue-shifted by 25 nm with respect to the weak emission band of **5**.

Similarly, the optical properties of **T₈-B₁₂** and **T₈-COSAN** were analysed through their UV–Vis absorption and PL spectra in CH_3CN (Table 1). The UV–Vis spectra of both POSS cages show their absorption maxima as a broadband in the range 270–272 nm, which is endorsed mainly to the styrene moieties [8,43]. Although this band is red-shifted with respect to free styrene (251 nm), this effect is in good agreement with the UV–Vis spectra of previously reported styrenyl-containing POSS with different spacers [8,88]. As described for compound **5**, the presence of COSAN units in **T₈-COSAN** is responsible for the additional absorption bands near 310 and 370 nm, as well as the weak absorption around 450–460 nm. Regarding the extinction coefficients, the COSAN cluster in **T₈-COSAN** increases the ϵ value with respect to **T₈-B₁₂** at their high energy absorption band (from 186,000 to 233,000), due to the nearness of the metallacarborane band at 310 nm. On the other hand, **T₈-B₁₂** and **T₈-COSAN** show nearly identical PL spectra, with emission maxima at $\lambda_{em} = 405\text{--}406$ nm after excitation at their maxima absorbance (Figure 2b, Table 1). This emission is in the range to that obtained for carborane-functionalised **T₈** through a styrene group ($\lambda_{em} = 370\text{--}414$ nm), but it is remarkably redshifted compared to the maximum emission ($\lambda_{em} = 326$ nm) of (*p*-methoxy-styrenyl)₈OS [88]. Therefore, the presence of either *closo*-dodecaborate or COSAN clusters as substituents in the styrenylOS cube seems to be responsible for this ~80 nm bathochromic shift. This could be due to a combination of phenomena, as the high electron delocalisation within the OS cube or possible interactions of the functional groups linked to the cage in the excited state [8,107]. In fact, the emission maxima of **T₈-B₁₂** and **T₈-COSAN** is even more redshifted than those observed for silsesquioxanes substituted with more conjugated systems, e.g., (stilbene-vinyl)₈OS emitting in a range $\lambda_{em} = 375\text{--}388$ nm in different solvents, (*p*-methyl-stilbene-vinyl)₈OS with $\lambda_{em} = 398$ nm [88,108], and even (carborane-vinylstilbene)₈OS hybrids with $\lambda_{em} = 391\text{--}392$ nm [7]. Regarding the PL quantum yield, CH_3CN solutions of **T₈-B₁₂** and **T₈-COSAN** were analysed. Differently to the equivalent (*p*-methoxy-styrenyl)₈OS core that shows a $\Phi_F = 12\%$ [88], the polyanionic **T₈** hybrids here prepared show low emission efficiencies, with values $\Phi_F = 1.4\text{--}1.8\%$. It is also worth noting that, in contrast to carborane-substituted **T₈**, either through styrene or vinyl-stilbene moieties [8,43], in this work there is no apparent relationship between the type of boron cluster and the emission efficiency behaviour. Nevertheless, it is evident that incorporation of anionic boron clusters to the POSS cube gives rise to low emissive materials in the solution.

2.3. Thermal Stability of Anionic-Boron Clusters Containing **T₈**

Silsesquioxanes have been used as additives in polymers and composites to improve their thermal, mechanical, and oxidative resistance [109,110]. Additionally, it has been stated that boron clusters have high thermal stability (*vide supra*). To study the influence of thermal behaviour when these two

families of compounds are combined, we reported the thermal stability of the T_8 -COSAN hybrid [43], and the thermogravimetric analysis (TGA) of T_8 - B_{12} under argon was here studied (Figure 3). The TGA results show a very different behaviour when nonfunctionalised OVS is compared to T_8 - B_{12} and T_8 -COSAN. Pristine OVS shows a sharp fall near 290 °C, and after heating up to 900 °C, 18% of the initial weight was recovered [111]. On the contrary, the boron cluster-containing OVS hybrids undergo a gradual weight reduction between 300–500 °C, and a residual mass of around 58% and 88% were respectively recovered, after heating up to 900 °C for T_8 - B_{12} and T_8 -COSAN, respectively. In T_8 - B_{12} the percentage of organic part is around 82%, whereas only 11% would correspond to the percentage of hydrogen. Therefore, after burning these materials, we may propose that the total of hydrogen and a percentage of the organic part (around 31%) are lost; being this percentage higher for T_8 - B_{12} with regards to T_8 -COSAN (around 4.4%). This result confirms once again that binding anionic boron clusters to the T_8 cube cause a significant increase in the thermal stability of the final materials; moreover, those materials containing metallocarborane fragments are the most thermally stable.

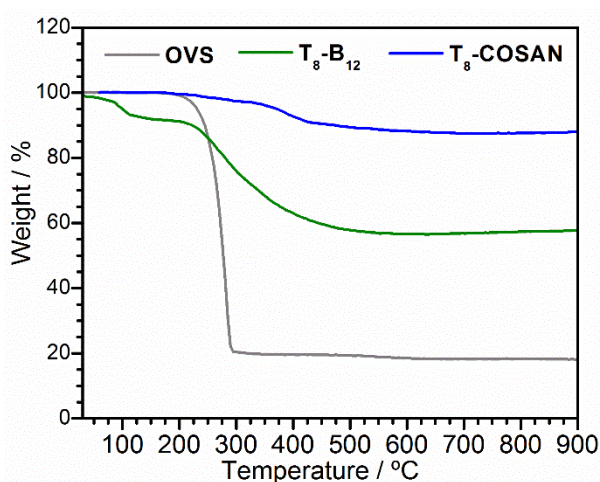


Figure 3. Thermogravimetric analysis (TGA) data under argon (10 °C/min) for octavinylsilsesquioxane (OVS), T_8 - B_{12} and T_8 -COSAN.

3. Materials and Methods

3.1. Materials

All reactions were performed under an atmosphere of dinitrogen employing standard Schlenk techniques. Acetonitrile and dichloromethane were purchased from Merck and distilled from sodium benzophenone before use. Commercial grade acetone, hexane, ethyl acetate, tetrahydrofuran, and methanol were used without further purification. Compounds $[Bu_4N][B_{12}H_{11}(C_4H_8O_2)]$ (2) [93] and $[3,3'-Co(8-C_4H_8O_2-1,2-C_2B_9H_{10})(1',2'-C_2B_9H_{11})]$ (3) [94] and T_8 -COSAN [43] were synthesised according to the literature. Compounds $[Bu_4N]Br$, Grubbs 1st generation catalyst $[RuCl_2(CHPh)-(PCy_3)_2]$, octavinylsilsesquioxane (OVS), 1,3,5-tris(4-hydroxyphenyl)benzene (1) and 4-vinylphenol solution 10 wt% in propylene glycol were purchased from Sigma-Aldrich (Merck Life Science, Madrid, Spain). K_2CO_3 was obtained from Labkem (Barcelona, Spain).

3.2. Instrumentation

Elemental analyses were performed using a Thermo (Carlo Erba) Flash 2000 Elemental Analyser microanalyzer (EA Consumables, Inc., Pennsauken, NJ, USA). ATR-IR spectra were recorded on a JASCO FT/IR-4700 spectrometer on a high-resolution (Madrid, Spain). The 1H -NMR (300.13 MHz), $^{11}B\{^1H\}$ (96.29 MHz), and $^{13}C\{^1H\}$ NMR (75.47 MHz) spectra were recorded on a Bruker ARX 300 spectrometer (Bellerica, MA, USA). All NMR spectra were recorded in CD_3COCD_3 solutions at 25 °C. Chemical shift values for $^{11}B\{^1H\}$ NMR spectra were referenced to external $BF_3 \cdot OEt_2$, and those for 1H

and $^{13}\text{C}\{^1\text{H}\}$ NMR were referenced to SiMe_4 (TMS). Chemical shifts are reported in units of parts per million downfield from the reference, and all coupling constants are reported in Hertz. UV–Vis spectra were recorded on a VARIANT Cary 5 UV–Vis–NIR spectrophotometer (Santa Clara, CA, USA), using a spectroscopic grade ACN (Sigma-Aldrich, Merck Life Science, Madrid, Spain), in normal quartz cuvette having 1 cm path length, for different solutions for each compound in the range 2×10^{-6} to 5×10^{-6} M in order to calculate the molar extinction coefficients (ϵ). The fluorescence emission spectra and excitation spectra for all samples were recorded in a VARIANT Cary Eclipse fluorescence spectrometer. No fluorescent contaminants were detected on excitation in the wavelength region of experimental interest. The fluorescence quantum yields were determined by the “single point method” and repeated three times with similar optical density for reproducibility [112], against quinine sulfate in a 0.5 M aqueous sulfuric acid with $\phi_F = 0.54$ as a standard [113].

3.3. Synthesis of Derivatives 4, 5, 6, and T₈-B₁₂

3.3.1. Synthesis of 4

A 5 mL round-bottomed flask was charged under nitrogen with **1** (5 mg, 0.014 mmol), **2** (20.90 mg, 0.044 mmol), K_2CO_3 (25 mg, 0.181 mmol), and $[\text{NBu}_4]\text{Br}$ (15.4 mg, 0.047 mmol) in 2 mL of anhydrous CH_3CN . The solution was stirred and refluxed overnight. After, the reaction mixture was washed with THF, filtered, and the solvent was removed under vacuum. Further purification was performed by preparative layer chromatography ($\text{CH}_2\text{Cl}_2/\text{CH}_3\text{CN}$, 1:1) to obtain compound **4** as white solid. Yield: 20 mg, 57%. ^1H NMR, δ (ppm): 7.72 (br, 6H, C_6H_4), 7.70 (s, 3H, C_6H_3), 7.08 (d, $^3J(\text{H,H}) = 9$ Hz, 6H, C_6H_4), 4.24 (t, $^3J(\text{H,H}) = 4.5$ Hz, 6H, $\text{CH}_2\text{-O}$), 3.94 (t, $^3J(\text{H,H}) = 4.5$ Hz, 6H, $\text{CH}_2\text{-O}$), 3.74 (br, 6H, $\text{CH}_2\text{-O}$), 3.69 (br, 6H, $\text{CH}_2\text{-O}$), 3.42 (t, $^3J(\text{H,H}) = 9$ Hz, 48H, N- CH_2), 1.85–1.75 (m, 48H, N- $\text{CH}_2\text{-CH}_2$), 1.51–1.39 (m, 48H, N- $\text{CH}_2\text{-CH}_2\text{-CH}_2$), 0.98 (t, $^3J(\text{H,H}) = 7.5$ Hz, 72H, N- $\text{CH}_2\text{-CH}_2\text{-CH}_2\text{-CH}_3$); $^{11}\text{B}\{^1\text{H}\}$ NMR, δ (ppm): 7.72 (s, 3B, B-O), -15.34 (s, 15B), -16.13 (s, 15B), -20.89 ppm (s, 3B); $^{13}\text{C}\{^1\text{H}\}$ NMR, δ (ppm): 159.94 (s; C_6H_4), 142.73 (s; C_6H_3), 134.38 (s, C_6H_4), 129.16 (s, C_6H_4), 124.02 (s; C_6H_3), 116.05 (s; C_6H_4), 73.96 (s; O- CH_2), 70.31 (s; O- CH_2), 68.93 (s; O- CH_2), 68.66 (s; O- CH_2), 59.59 (s, N CH_2), 24.68 (s, $\text{CH}_3\text{CH}_2\text{CH}_2$), 20.50 (s, $\text{CH}_3\text{CH}_2\text{CH}_2$), 14.06 (s, CH_3); ATR-IR (cm^{-1}): $\nu = 2959, 2931, 2871$ ($\text{C}_{\text{ar}}\text{H}$), 2466 (B-H), 1606 (C=C), 1470 (N-C).

3.3.2. Synthesis of 5

A solution of **1** (68 mg, 0.193 mmol) and NaH (57.7% dispersion, 28 mg, 0.66 mmol) in 5 mL of dry THF was stirred under nitrogen for 1 h at room temperature. Then, **3** (250 mg, 0.61 mmol) was added and the mixture was refluxed for 60 h. The reaction was cooled down and quenched with CH_3OH (1 mL), water (3 mL), and a few drops of acetic acid (1 M). The organic solvents were removed under vacuum, and the crude product was dissolved in 10 mL diethyl ether and extracted with water (3×10 mL). The organic layer was dried over MgSO_4 and the volatiles were reduced under vacuum. Further purification was performed with preparative layer chromatography ($\text{CH}_2\text{Cl}_2/\text{CH}_3\text{CN}$, 8:2) to obtain **5** as an orange solid. Yield: 201 mg, 63%. ^1H -NMR, δ (ppm): 7.80 (br, 6H; C_6H_4), 7.78 (s, 3H, C_6H_3), 7.11 (d, $^3J(\text{H,H}) = 8$ Hz, 2H, C_6H_4), 4.32 (br, 6H, $\text{C}_c\text{-H}$), 4.29 (br, 6H, $\text{C}_c\text{-H}$), 4.23 (t, $^3J(\text{H,H}) = 4$ Hz, 6H, O CH_2), 3.88 (t, $^3J(\text{H,H}) = 4$ Hz, 6H, O CH_2), 3.65–3.62 (m, 12H, O CH_2); $^{11}\text{B}\{^1\text{H}\}$ NMR, δ (ppm): 24.32 (s, 3B, B-O), 5.35 (s, 3B, B-H), 1.74 (s, 3B, B-H), -1.14 (s, 3B, B-H), -2.97 (s, 6B, B-H), -6.08 (s, 9B, B-H), -6.82 (s, 9B, B-H), -15.95 (s, 6B, B-H), -19.10 (br, 9B, B-H), -27.08 (s, 3B, B-H); $^{13}\text{C}\{^1\text{H}\}$ NMR, δ (ppm): 159.68 (s; C_6H_4), 142.57 (s; C_6H_3), 134.31 (s, C_6H_4), 129.01 (s, C_6H_4), 123.92 (s; C_6H_3), 115.73 (s; C_6H_4), 72.80 (s; O- CH_2), 70.19 (s; O- CH_2), 69.20 (s; O- CH_2), 68.39 (s; O- CH_2), 55.22 (s, $\text{C}_c\text{-H}$), 47.20 (s, $\text{C}_c\text{-H}$); ATR-IR (cm^{-1}): $\tilde{\nu} = 3039$ ($\text{C}_c\text{-H}$), 2924, 2874 ($\text{C}_{\text{ar}}\text{H}$), 2534 (B-H), 1606 (C=C); elemental analysis calcd. (%) for $\text{C}_{48}\text{H}_{102}\text{B}_{54}\text{C}_3\text{O}_3\text{Na}_3\text{O}_9$: C, 34.88; H, 6.22. Found: C, 34.72; H, 6.53.

3.3.3. Synthesis of **6**

A mixture of **2** (250 mg, 0.531 mmol), K_2CO_3 (293 mg, 2.12 mmol), 4-vinylphenol solution (0.62 mL, 0.535 mmol), $[NBu_4]Br$ (172 mg, 0.531 mmol), and 10 mL of anhydrous acetonitrile under nitrogen was refluxed overnight in a 25 mL round-bottomed flask. The reaction mixture was filtered off and the solvent was removed under vacuum. The brown oil was dissolved in 10 mL of CH_2Cl_2 and extracted with water (3×10 mL). The organic layer was dried over $MgSO_4$ and the volatiles were reduced under vacuum. Further purification was performed by a silica gel column chromatography (ethyl acetate/hexane, 1:1) to obtain compound **6** as a brownish oil. Yield: 317 mg, 72%. 1H NMR, δ (ppm): 7.40 (d, $^3J(H,H) = 9$ Hz, 2H, C_6H_4), 6.97 (d, $^3J(H,H) = 9$ Hz, 2H, C_6H_4), 6.69 (dd, $^3J(H,H) = 18$ Hz, $^3J(H,H) = 12$ Hz, 1H, $CH=CH_2$), 5.65 (d, $^3J(H,H) = 18$ Hz, 1H, $CH=CH_2$), 5.08 (d, $^3J(H,H) = 12$ Hz, 1H, $CH=CH_2$), 4.19 (t, $^3J(H,H) = 4.5$ Hz, 2H, CH_2-O), 3.86 (t, $^3J(H,H) = 4.5$ Hz, 2H, CH_2-O), 3.69 (br, 2H, CH_2-O), 3.62 (br, 2H, CH_2-O), 3.43 (t, $^3J(H,H) = 7.5$ Hz, 16H, N- CH_2), 1.87–1.76 (m, 16H, N- CH_2-CH_2), 1.52–1.40 (m, 16H, N- $CH_2-CH_2-CH_2$), 0.99 (t, $^3J(H,H) = 7.5$ Hz, 24H, N- $CH_2-CH_2-CH_2-CH_3$); $^{11}B\{^1H\}$ NMR, δ (ppm): 7.43 (s, 1B, B-O), -15.51 (s, 5B), -16.10 (s, 5B), -21.08 ppm (s, 1B); $^{13}C\{^1H\}$ NMR, δ (ppm): 159.15 (s, C-O), 136.49 (s, CH- C_6H_4), 130.18 (s, CH- C_6H_4), 127.33 (s, C_6H_4), 114.66 (s, C_6H_4), 110.61 (s, $CH=CH_2$), 73.13 (s, CH_2-O), 69.22 (s, CH_2-O), 67.90 (s, CH_2-O), 67.90 (s, CH_2-O), 58.63 (s, N- CH_2), 23.74 (s, N- CH_2-CH_2), 19.51 (s, N- $CH_2-CH_2-CH_2$), 13.10 (s, N- $CH_2-CH_2-CH_2-CH_3$); ATR-IR (cm^{-1}): $\nu = 2462$ (s, B-H st), 1600 (m, C=C st); elemental analysis calcd. (%) for $C_{44}H_{98}B_{12}N_2O_3$ (+3.5 H_2O + 0.5 CH_2Cl_2 + 1 AcOEt): C, 56.74; H, 11.19; N, 2.73. Found: C, 56.70; H, 11.09; N, 2.69.

3.3.4. Synthesis of **T₈-B₁₂**

A 10 mL round-bottomed flask was charged under nitrogen with **OVS** (15 mg, 0.024 mmol), compound **6** (190 mg, 0.227 mmol), and the first generation Grubbs catalyst (12 mg, 0.014 mmol) in 6 mL of CH_2Cl_2 . The solution was stirred and refluxed for three days. The solvent was removed under vacuum. The residue was treated with a mixture of THF/MeOH (1:10) to obtain a grey solid. Further purification was performed by preparative layer chromatography (acetone/hexane, 7:3) to obtain compound **T₈-B₁₂** as a white solid. Yield: 32 mg, 18%. 1H NMR, δ (ppm): 7.54 (d, $^3J(H,H) = 6$ Hz, 16H, C_6H_4), 7.39 (d, $^3J(H,H) = 18$ Hz, 8H, $CH=CH-Si$), 7.02 (d, $^3J(H,H) = 9$ Hz, 6H, C_6H_4), 6.26 (d, $^3J(H,H) = 18$ Hz, 8H, $CH=CH-Si$), 4.23 (br, 16H, CH_2-O), 3.91 (br, 16H, CH_2-O), 3.72 (br, 16H, CH_2-O), 3.66 (br, 16H, CH_2-O), 3.38 (t, $^3J(H,H) = 9$ Hz, 128H, N- CH_2), 1.82–1.72 (m, 128H, N- CH_2-CH_2), 1.50–1.38 (m, 128H, N- $CH_2-CH_2-CH_2$), 0.98 (t, $^3J(H,H) = 6$ Hz, 192H, N- $CH_2-CH_2-CH_2-CH_3$); $^{11}B\{^1H\}$ NMR, δ (ppm): 7.76 (br, 8B, B-O), -15.29 (s, 40B), -16.15 (s, 40B), -20.91 ppm (br, 8B); $^{13}C\{^1H\}$ NMR, δ (ppm): 160.20 (s, C-O), 148.93 (s, CH- C_6H_4), 129.87 (s, CH- C_6H_4), 128.46 (s, C_6H_4), 114.89 (s, C_6H_4), 114.00 (s, Si- $CH=CH$), 73.10 (s, CH_2-O), 69.32 (s, CH_2-O), 68.08 (s, CH_2-O), 67.92 (s, CH_2-O), 58.53 (s, N- CH_2), 23.71 (s, N- CH_2-CH_2), 19.53 (s, N- $CH_2-CH_2-CH_2$), 13.20 (s, N- $CH_2-CH_2-CH_2-CH_3$); ATR-IR (cm^{-1}): $\nu = 2959, 2932, 2872$ ($C_{ar}H$), 2466 (B-H), 1602 (C=C), 1479 (N-C), 1091 (Si-O).

4. Conclusions

A set of 1,3,5-triphenylbenzene and octasilsesquioxane-based hybrids decorated with three (**4**, **5**) and eight *closo*-decahydro-dodecaborate and cobaltabisdicarbollide (**T₈-B₁₂**, **T₈-COSAN**), respectively, have been successfully synthesised, isolated, and fully characterised. Although they possess different types of fluorophores, all of them show a similar maxima absorption wavelength, which is red-shifted with regard to the nonsubstituted scaffolds. The molar extinction coefficient is correlated with the type of boron cluster, and proportional to the number of clusters attached to the core molecules. It is worth noting that a significant red-shift of the emission maxima (λ_{em} 369–406 nm) up to 80 nm for the **T₈** hybrids, as well as an important drop of the fluorescence efficiencies were produced after linking these anionic boron clusters to both scaffolds. These results confirm once again that the B_{12} and COSAN clusters produce a significant quenching of the fluorescence in the solution. Notably, binding anionic boron clusters to the OVS provide materials with an extraordinary thermal stability.

Supplementary Materials: The following are available online, Figure S1: Structure of compound **T₈-COSAN**; Figure S2: ¹H NMR (acetone-d₆, 300 MHz) of **4**; Figure S3: ¹¹B{¹H} NMR (acetone-d₆, 300 MHz) of **4**; Figure S4: ¹³C{¹H} NMR (acetone-d₆, 300 MHz) of **4**; Figure S5: ¹H NMR (acetone-d₆, 300 MHz) of **5**; Figure S6: ¹¹B{¹H} NMR (acetone-d₆, 300 MHz) of **5**; Figure S7: ¹³C{¹H} NMR (acetone-d₆, 300 MHz) of **5**; Figure S8: ¹H NMR (acetone-d₆, 300 MHz) of **6**; Figure S9: ¹¹B{¹H} NMR (acetone-d₆, 300 MHz) of **6**; Figure S10: ¹³C{¹H} NMR (acetone-d₆, 300 MHz) of **6**; Figure S11: ¹H NMR (acetone-d₆, 300 MHz) of **T₈-B₁₂**; Figure S12: ¹¹B{¹H} NMR (acetone-d₆, 300 MHz) of **T₈-B₁₂**; Figure S13: ¹³C{¹H} NMR (acetone-d₆, 300 MHz) of **T₈-B₁₂**; Figure S14: FTIR-ATR spectrum of **4**; Figure S15: FTIR-ATR spectrum of **5**; Figure S16: FTIR-ATR spectrum of **6**; Figure S17: FTIR-ATR spectrum of **T₈-B₁₂**.

Author Contributions: Manuscript conception, R.N.; writing and original draft preparation, R.N. and J.C.-G.; synthesis of derivatives **4**, **5**, **6**, and **T₈-B₁₂**, J.C.-G.; photophysical and thermal analysis, M.C.; editing, data analysis, and interpretation, J.C.-G., M.C., F.T., C.V., and R.N. All authors have read and agreed to the published version of the manuscript.

Funding: This research was funded by the MINECO grant CTQ2016-75150-R and Generalitat de Catalunya (2017/SGR/1720).

Acknowledgments: J.C.-G., M.C., F.T., C.V., and R.N. thank the MINECO grant CTQ2016-75150-R and Generalitat de Catalunya (2017/SGR/1720) for financial support. ICMAB acknowledges the support of the Spanish MINECO through the Severo Ochoa Centers of Excellence Program, under grant SEV-2015-0496.

Conflicts of Interest: The authors declare no conflict of interest. The funders had no role in the design of the study; in the collection, analyses, or interpretation of data; in the writing of the manuscript, or in the decision to publish the results.

References

1. Núñez, R.; Tarrès, M.; Ferrer-Ugalde, A.; Fabrizi de Biani, F.; Teixidor, F. Electrochemistry and Photoluminescence of Icosahedral Carboranes, Boranes, Metallocarboranes, and Their Derivatives. *Chem. Rev.* **2016**, *116*, 14307–14378. [[CrossRef](#)] [[PubMed](#)]
2. Mukherjee, S.; Thilagar, P. Boron clusters in luminescent materials. *Chem. Commun.* **2016**, *52*, 1070–1093. [[CrossRef](#)] [[PubMed](#)]
3. Poater, J.; Solà, M.; Viñas, C.; Teixidor, F. π Aromaticity and Three-Dimensional Aromaticity: Two sides of the Same Coin? *Angew. Chem. Int. Ed.* **2014**, *53*, 12191–12195. [[CrossRef](#)] [[PubMed](#)]
4. Poater, J.; Solà, M.; Viñas, C.; Teixidor, F. Back Cover: A Simple Link between Hydrocarbon and Borohydride Chemistries. *Chem. Eur. J.* **2013**, *19*, 4372. [[CrossRef](#)]
5. Kahlert, J.; Stammer, H.-G.; Neumann, B.; Harder, R.A.; Weber, L.; Fox, M.A. Crystal Structures of the Carborane Dianions [1,4-(PhCB10H10C)2C6H4]2⁻ and [1,4-(PhCB10H10C)2C6F4]2⁻ and the Stabilizing Role of the para-Phenylene Unit on 2n+3 Skeletal Electron Clusters. *Angew. Chem.* **2014**, *126*, 3776–3779. [[CrossRef](#)]
6. Sillanpää, R.; Kivekas, R.; Teixidor, F.; Viñas, C.; Núñez, R. 1-Diisopropylphosphino-2-phenyl-1,2-dicarba-closo-dodecaborane(12). *Acta Crystallogr.* **1996**, *52*, 2223–2225. [[CrossRef](#)]
7. Cabrera-Gonzalez, J.; Ferrer-Ugalde, A.; Bhattacharyya, S.; Chaari, M.; Teixidor, F.; Gierschner, J.; Núñez, R. Fluorescent carborane-vinylstilbene functionalised octasilsesquioxanes: Synthesis, structural, thermal and photophysical properties. *J. Mater. Chem. C* **2017**, *5*, 10211–10219. [[CrossRef](#)]
8. Ferrer-Ugalde, A.; Juárez-Pérez, E.J.; Teixidor, F.; Viñas, C.; Núñez, R. Synthesis, Characterization, and Thermal Behavior of Carboranyl–Styrene Decorated Octasilsesquioxanes: Influence of the Carborane Clusters on Photoluminescence. *Chem. Eur. J.* **2013**, *19*, 17021–17030. [[CrossRef](#)]
9. González-Campo, A.; Ferrer-Ugalde, A.; Viñas, C.; Teixidor, F.; Sillanpää, R.; Rodríguez-Romero, J.; Santillan, R.; Farfán, N.; Núñez, R. A Versatile Methodology for the Controlled Synthesis of Photoluminescent High-Boron-Content Dendrimers. *Chem. Eur. J.* **2013**, *19*, 6299–6312. [[CrossRef](#)]
10. Scholz, M.; Hey-Hawkins, E. Carbaboranes as Pharmacophores: Properties, Synthesis, and Application Strategies. *Chem. Rev.* **2011**, *111*, 7035–7062. [[CrossRef](#)]
11. Issa, F.; Kassiou, M.; Rendina, L.M. Boron in Drug Discovery: Carboranes as Unique Pharmacophores in Biologically Active Compounds. *Chem. Rev.* **2011**, *111*, 5701–5722. [[CrossRef](#)] [[PubMed](#)]

12. Řezáčová, P.; Pokorná, J.; Brynda, J.; Kožíšek, M.; Cígler, P.; Lepšík, M.; Fanfrlík, J.; Řezáč, J.; Grantz Šašková, K.; Siegllová, I.; et al. Design of HIV Protease Inhibitors Based on Inorganic Polyhedral Metallocarboranes. *J. Med. Chem.* **2009**, *52*, 7132–7141. [[CrossRef](#)] [[PubMed](#)]
13. Sivaev, I.B.; Bregadze, V.V. Polyhedral Boranes for Medical Applications: Current Status and Perspectives. *Eur. J. Inorg. Chem.* **2009**, *2009*, 1433–1450. [[CrossRef](#)]
14. Kožíšek, M.; Cígler, P.; Lepšík, M.; Fanfrlík, J.; Řezáčová, P.; Brynda, J.; Pokorná, J.; Plešek, J.; Grüner, B.; Grantz Šašková, K.; et al. Inorganic Polyhedral Metallocarborane Inhibitors of HIV Protease: A New Approach to Overcoming Antiviral Resistance. *J. Med. Chem.* **2008**, *51*, 4839–4843. [[CrossRef](#)]
15. Cígler, P.; Kožíšek, M.; Řezáčová, P.; Brynda, J.; Otwinowski, Z.; Pokorná, J.; Plešek, J.; Grüner, B.; Dolečková-Marešová, L.; Máša, M.; et al. From nonpeptide toward noncarbon protease inhibitors: Metallocarboranes as specific and potent inhibitors of HIV protease. *PNAS* **2005**, *102*, 15394–15399. [[CrossRef](#)]
16. Valliant, J.F.; Guenther, K.J.; King, A.S.; Morel, P.; Schaffer, P.; Sogbein, O.O.; Stephenson, K.A. The medicinal chemistry of carboranes. *Coord. Chem. Rev.* **2002**, *232*, 173–230. [[CrossRef](#)]
17. Hawthorne, M.F.; Maderna, A. Applications of Radiolabeled Boron Clusters to the Diagnosis and Treatment of Cancer. (Chem. Rev. **1999**, *99*, 3421–3434. Published on the Web Nov. 13, 1999). *Chem. Rev.* **2000**, *100*, 1165. [[CrossRef](#)]
18. Wu, X.; Guo, J.; Jia, W.; Zhao, J.; Jia, D.; Shan, H. Highly-efficient solid-state emission of tethered anthracene-o-carborane dyads and their visco- and thermo-chromic luminescence properties. *Dyes and Pigments* **2019**, *162*, 855–862. [[CrossRef](#)]
19. Wu, X.; Guo, J.; Quan, Y.; Jia, W.; Jia, D.; Chen, Y.; Xie, Z. Cage carbon-substitute does matter for aggregation-induced emission features of o-carborane-functionalized anthracene triads. *J. Mater. Chem. C* **2018**, *6*, 4140–4149. [[CrossRef](#)]
20. Wu, X.; Guo, J.; Cao, Y.; Zhao, J.; Jia, W.; Chen, Y.; Jia, D. Mechanically triggered reversible stepwise tricolor switching and thermochromism of anthracene-o-carborane dyad. *Chem. Sci.* **2018**, *9*, 5270–5277. [[CrossRef](#)]
21. Tu, D.; Leong, P.; Guo, S.; Yan, H.; Lu, C.; Zhao, Q. Highly Emissive Organic Single-Molecule White Emitters by Engineering o-Carborane-Based Luminophores. *Angew. Chem. Int. Ed.* **2017**, *56*, 11370–11374. [[CrossRef](#)] [[PubMed](#)]
22. Naito, H.; Nishino, K.; Morisaki, Y.; Tanaka, K.; Chujo, Y. Highly-efficient solid-state emissions of anthracene-o-carborane dyads with various substituents and their thermochromic luminescence properties. *J. Mater. Chem. C* **2017**, *5*, 10047–10054. [[CrossRef](#)]
23. Naito, H.; Nishino, K.; Morisaki, Y.; Tanaka, K.; Chujo, Y. Solid-State Emission of the Anthracene-o-Carborane Dyad from the Twisted-Intramolecular Charge Transfer in the Crystalline State. *Angew. Chem. Int. Ed.* **2017**, *56*, 254–259. [[CrossRef](#)] [[PubMed](#)]
24. Tu, D.; Leong, P.; Li, Z.; Hu, R.; Shi, C.; Zhang, K.Y.; Yan, H.; Zhao, Q. A carborane-triggered metastable charge transfer state leading to spontaneous recovery of mechanochromic luminescence. *Chem. Commun.* **2016**, *52*, 12494–12497. [[CrossRef](#)]
25. Kim, Y.; Park, S.; Lee, Y.H.; Jung, J.; Yoo, S.; Lee, M.H. Homoleptic Tris-Cyclometalated Iridium Complexes with Substituted o-Carboranes: Green Phosphorescent Emitters for Highly Efficient Solution-Processed Organic Light-Emitting Diodes. *Inorg. Chem.* **2016**, *55*, 909–917. [[CrossRef](#)]
26. Furue, R.; Nishimoto, T.; Park, I.S.; Lee, J.; Yasuda, T. Aggregation-Induced Delayed Fluorescence Based on Donor/Acceptor-Tethered Janus Carborane Triads: Unique Photophysical Properties of Nondoped OLEDs. *Angew. Chem. Int. Ed.* **2016**, *55*, 7171–7175. [[CrossRef](#)]
27. Kahlert, J.; Bohling, L.; Brockhinke, A.; Stammer, H.-G.; Neumann, B.; Rendina, L.M.; Low, P.J.; Weber, L.; Fox, M.A. Syntheses and reductions of C-dimesitylboryl-1,2-dicarba-closo-dodecaboranes. *Dalton Trans.* **2015**, *44*, 9766–9781. [[CrossRef](#)]
28. Naito, H.; Morisaki, Y.; Chujo, Y. o-Carborane-Based Anthracene: A Variety of Emission Behaviors. *Angew. Chem. Int. Ed.* **2015**, *54*, 5084–5087. [[CrossRef](#)]
29. Zhu, L.; Lv, W.; Liu, S.; Yan, H.; Zhao, Q.; Huang, W. Carborane enhanced two-photon absorption of tribranched fluorophores for fluorescence microscopy imaging. *Chem. Commun.* **2013**, *49*, 10638–10640. [[CrossRef](#)]
30. Wee, K.-R.; Cho, Y.-J.; Jeong, S.; Kwon, S.; Lee, J.-D.; Suh, I.-H.; Kang, S.O. Carborane-Based Optoelectronically Active Organic Molecules: Wide Band Gap Host Materials for Blue Phosphorescence. *J. Am. Chem. Soc.* **2012**, *134*, 17982–17990. [[CrossRef](#)]

31. Chaari, M.; Kelemen, Z.; Choquesillo-Lazarte, D.; Gaztelumendi, N.; Teixidor, F.; Viñas, C.; Nogués, C.; Núñez, R. Efficient blue light emitting materials based on m-carborane–anthracene dyads. Structure, photophysics and bioimaging studies. *Biomater. Sci.* **2019**, *7*, 5324–5337. [[CrossRef](#)] [[PubMed](#)]
32. Bellomo, C.; Chaari, M.; Cabrera-González, J.; Blangetti, M.; Lombardi, C.; Deagostino, A.; Viñas, C.; Gaztelumendi, N.; Nogués, C.; Nuñez, R.; et al. Carborane-BODIPY Dyads: New Photoluminescent Materials through an Efficient Heck Coupling. *Chem. Eur. J.* **2018**, *24*, 15622–15630. [[CrossRef](#)] [[PubMed](#)]
33. Chaari, M.; Cabrera-González, J.; Kelemen, Z.; Viñas, C.; Ferrer-Ugalde, A.; Choquesillo-Lazarte, D.; Ben Salah, A.; Teixidor, F.; Núñez, R. Luminescence properties of carborane-containing distyrylaromatic systems. *J. Organomet. Chem.* **2018**, *865*, 206–213. [[CrossRef](#)]
34. Chaari, M.; Kelemen, Z.; Planas, J.G.; Teixidor, F.; Choquesillo-Lazarte, D.; Ben Salah, A.; Viñas, C.; Núñez, R. Photoluminescence in m-carborane–anthracene triads: A combined experimental and computational study. *J. Mater. Chem. C* **2018**, *6*, 11336–11347. [[CrossRef](#)]
35. Ferrer-Ugalde, A.; Cabrera-González, J.; Juárez-Pérez, E.J.; Teixidor, F.; Pérez-Inestrosa, E.; Montenegro, J.M.; Sillanpää, R.; Haukka, M.; Núñez, R. Carborane–stilbene dyads: The influence of substituents and cluster isomers on photoluminescence properties. *Dalton Trans.* **2017**, *46*, 2091–2104. [[CrossRef](#)]
36. Cabrera-González, J.; Bhattacharyya, S.; Milián-Medina, B.; Teixidor, F.; Farfán, N.; Arcos-Ramos, R.; Vargas-Reyes, V.; Gierschner, J.; Núñez, R. Tetrakis[(p-dodecacarboranyl)methyl]stilbenyl}ethylene: A Luminescent Tetraphenylethylene (TPE) Core System. *Eur. J. Inorg. Chem.* **2017**, *2017*, 4575–4580. [[CrossRef](#)]
37. Cabrera-González, J.; Viñas, C.; Haukka, M.; Bhattacharyya, S.; Gierschner, J.; Núñez, R. Photoluminescence in Carborane–Stilbene Triads: A Structural, Spectroscopic, and Computational Study. *Chem. Eur. J.* **2016**, *22*, 13588–13598. [[CrossRef](#)]
38. Ferrer-Ugalde, A.; González-Campo, A.; Viñas, C.; Rodríguez-Romero, J.; Santillan, R.; Farfán, N.; Sillanpää, R.; Sousa-Pedrares, A.; Núñez, R.; Teixidor, F. Fluorescence of New o-Carborane Compounds with Different Fluorophores: Can it be Tuned? *Chem. Eur. J.* **2014**, *20*, 9940–9951. [[CrossRef](#)]
39. Ferrer-Ugalde, A.; Juárez-Pérez, E.J.; Teixidor, F.; Viñas, C.; Sillanpää, R.; Pérez-Inestrosa, E.; Núñez, R. Synthesis and Characterization of New Fluorescent Styrene-Containing Carborane Derivatives: The Singular Quenching Role of a Phenyl Substituent. *Chem. Eur. J.* **2012**, *18*, 544–553. [[CrossRef](#)]
40. Tarrès, M.; Arderiu, V.S.; Zaulet, A.; Viñas, C.; Fabrizi de Biani, F.; Teixidor, F. How to get the desired reduction voltage in a single framework! Metallacarborane as an optimal probe for sequential voltage tuning. *Dalton Trans.* **2015**, *44*, 11690–11695. [[CrossRef](#)]
41. Lupu, M.; Zaulet, A.; Teixidor, F.; Ruiz, E.; Viñas, C. Negatively Charged Metallacarborane Redox Couples with Both Members Stable to Air. *Chem. Eur. J.* **2015**, *21*, 6888–6897. [[CrossRef](#)] [[PubMed](#)]
42. Pepiol, A.; Teixidor, F.; Sillanpää, R.; Lupu, M.; Viñas, C. Stepwise Sequential Redox Potential Modulation Possible on a Single Platform. *Angew. Chem. Int. Ed.* **2011**, *50*, 12491–12495. [[CrossRef](#)] [[PubMed](#)]
43. Cabrera-González, J.; Sánchez-Arderiu, V.; Viñas, C.; Parella, T.; Teixidor, F.; Núñez, R. Redox-Active Metallacarborane-Decorated Octasilsesquioxanes. Electrochemical and Thermal Properties. *Inorg. Chem.* **2016**, *55*, 11630–11634. [[CrossRef](#)] [[PubMed](#)]
44. Cabrera-González, J.; Cabana, L.; Ballesteros, B.; Tobias, G.; Núñez, R. Highly Dispersible and Stable Anionic Boron Cluster–Graphene Oxide Nanohybrids. *Chem. Eur. J.* **2016**, *22*, 5096–5101. [[CrossRef](#)]
45. Grüner, B.; Rais, J.; Selucký, P.; Lucaníková, M. Recent Progress in Extraction Agents Based on Cobalt Bis(Dicarbollides) for Partitioning of Radionuclides from High-Level Nuclear Waste. In *Boron Science: New Technologies and Applications*; Hosmane, N.S., Ed.; Taylor & Francis: Boca Roca, FL, USA, 2012; pp. 463–490.
46. Masalles, C.; Llop, J.; Viñas, C.; Teixidor, F. Extraordinary Overoxidation Resistance Increase in Self-Doped Polypyrroles by Using Non-conventional Low Charge-Density Anions. *Adv. Mater.* **2002**, *14*, 826–829. [[CrossRef](#)]
47. Fernández-Alvarez, R.; Ďord'ovič, V.; Uchman, M.; Matějček, P. Amphiphiles without Head-and-Tail Design: Nanostructures Based on the Self-Assembly of Anionic Boron Cluster Compounds. *Langmuir* **2018**, *34*, 3541–3554. [[CrossRef](#)]
48. Gassin, P.-M.; Girard, L.; Martin-Gassin, G.; Brusselle, D.; Jonchère, A.; Diat, O.; Viñas, C.; Teixidor, F.; Bauduin, P. Surface Activity and Molecular Organization of Metallacarboranes at the Air–Water Interface Revealed by Nonlinear Optics. *Langmuir* **2015**, *31*, 2297–2303. [[CrossRef](#)]

49. Uchman, M.; Ďord'ovič, V.; Tošner, Z.; Matějček, P. Classical Amphiphilic Behavior of Nonclassical Amphiphiles: A Comparison of Metallacarborane Self-Assembly with SDS Micellization. *Angew. Chem. Int. Ed.* **2015**, *54*, 14113–14117. [[CrossRef](#)]
50. Verdía-Báguena, C.; Alcaraz, A.; Aguilera, V.M.; Cioran, A.M.; Tachikawa, S.; Nakamura, H.; Teixidor, F.; Viñas, C. Amphiphilic COSAN and I₂-COSAN crossing synthetic lipid membranes: Planar bilayers and liposomes. *Chem. Commun.* **2014**, *50*, 6700–6703. [[CrossRef](#)]
51. Brusselle, D.; Bauduin, P.; Girard, L.; Zaulet, A.; Viñas, C.; Teixidor, F.; Ly, I.; Diat, O. Lyotropic Lamellar Phase Formed from Monolayered θ -Shaped Carborane-Cage Amphiphiles. *Angew. Chem. Int. Ed.* **2013**, *52*, 12114–12118. [[CrossRef](#)]
52. Rak, J.; Dejlová, B.; Lampová, H.; Kaplánek, R.; Matějček, P.; Cígler, P.; Král, V. On the Solubility and Lipophilicity of Metallacarborane Pharmacophores. *Mol. Pharm.* **2013**, *10*, 1751–1759. [[CrossRef](#)] [[PubMed](#)]
53. Bauduin, P.; Prevost, S.; Farràs, P.; Teixidor, F.; Diat, O.; Zemb, T. A Theta-Shaped Amphiphilic Cobaltabisdicarbollide Anion: Transition From Monolayer Vesicles to Micelles. *Angew. Chem. Int. Ed.* **2011**, *50*, 5298–5300. [[CrossRef](#)] [[PubMed](#)]
54. Fuentes, I.; García-Mendiola, T.; Sato, S.; Pita, M.; Nakamura, H.; Lorenzo, E.; Teixidor, F.; Marques, F.; Viñas, C. Metallacarboranes on the Road to Anticancer Therapies: Cellular Uptake, DNA Interaction, and Biological Evaluation of Cobaltabisdicarbollide [COSAN][−]. *Chem. Eur. J.* **2018**, *24*, 17239–17254. [[CrossRef](#)] [[PubMed](#)]
55. Zheng, Y.; Liu, W.; Chen, Y.; Jiang, H.; Yan, H.; Kosenko, I.; Chekulaeva, L.; Sivaev, I.; Bregadze, V.; Wang, X. A Highly Potent Antibacterial Agent Targeting Methicillin-Resistant Staphylococcus aureus Based on Cobalt Bis(1,2-Dicarbollide) Alkoxy Derivative. *Organometallics* **2017**, *36*, 3484–3490. [[CrossRef](#)]
56. Goszczyński, T.M.; Fink, K.; Kowalski, K.; Leśnikowski, Z.J.; Boratyński, J. Interactions of Boron Clusters and their Derivatives with Serum Albumin. *Sci. Rep.* **2017**, *7*, 9800. [[CrossRef](#)]
57. García-Mendiola, T.; Bayon-Pizarro, V.; Zaulet, A.; Fuentes, I.; Pariente, F.; Teixidor, F.; Viñas, C.; Lorenzo, E. Metallacarboranes as tunable redox potential electrochemical indicators for screening of gene mutation. *Chem. Sci.* **2016**, *7*, 5786–5797. [[CrossRef](#)]
58. Leśnikowski, Z.J. Challenges and Opportunities for the Application of Boron Clusters in Drug Design. *J. Med. Chem.* **2016**, *59*, 7738–7758. [[CrossRef](#)]
59. Tarrés, M.; Canetta, E.; Paul, E.; Forbes, J.; Azzouni, K.; Viñas, C.; Teixidor, F.; Harwood, A.J. Biological interaction of living cells with COSAN-based synthetic vesicles. *Sci. Rep.* **2015**, *5*, 7804. [[CrossRef](#)]
60. Viñas, C. The uniqueness of boron as a novel challenging element for drugs in pharmacology, medicine and for smart biomaterials. *Future Med. Chem.* **2013**, *5*, 617–619. [[CrossRef](#)]
61. Sivaev, I.B.; Bregadze, V.I.; Sjöberg, S. Chemistry of closo-Dodecaborate Anion [B₁₂H₁₂]^{2−}: A Review. *Collect. Czech. Chem. Commun.* **2002**, *67*, 679–727. [[CrossRef](#)]
62. Karki, K.; Gabel, D.; Roccatano, D. Structure and Dynamics of Dodecaborate Clusters in Water. *Inorg. Chem.* **2012**, *51*, 4894–4896. [[CrossRef](#)] [[PubMed](#)]
63. Assaf, K.I.; Ural, M.S.; Pan, F.; Georgiev, T.; Simova, S.; Rissanen, K.; Gabel, D.; Nau, W.M. Water Structure Recovery in Chaotropic Anion Recognition: High-Affinity Binding of Dodecaborate Clusters to γ -Cyclodextrin. *Angew. Chem. Int. Ed.* **2015**, *54*, 6852–6856. [[CrossRef](#)] [[PubMed](#)]
64. Viñas, C.; Tarrés, M.; González-Cardoso, P.; Farràs, P.; Bauduin, P.; Teixidor, F. Surfactant behaviour of metallacarboranes. A study based on the electrolysis of water. *Dalton Trans.* **2014**, *43*, 5062–5068. [[CrossRef](#)] [[PubMed](#)]
65. Tachikawa, S.; Miyoshi, T.; Koganei, H.; El-Zaria, M.E.; Viñas, C.; Suzuki, M.; Ono, K.; Nakamura, H. Spermidinium closo-dodecaborate-encapsulating liposomes as efficient boron delivery vehicles for neutron capture therapy. *Chem. Commun.* **2014**, *50*, 12325–12328. [[CrossRef](#)] [[PubMed](#)]
66. Ishii, S.; Sato, S.; Asami, H.; Hasegawa, T.; Kohno, J.-Y.; Nakamura, H. Design of S–S bond containing maleimide-conjugated closo-dodecaborate (SSMID): Identification of unique modification sites on albumin and investigation of intracellular uptake. *Org. Biomol. Chem.* **2019**, *17*, 5496–5499. [[CrossRef](#)]
67. Ishii, S.; Nakamura, H. Synthesis and biological evaluation of closo-dodecaborate ibuprofen conjugate (DIC) as a new boron agent for neutron capture therapy. *J. Organomet. Chem.* **2018**, *865*, 178–182. [[CrossRef](#)]
68. Awad, D.; Bartok, M.; Mostaghimi, F.; Schrader, I.; Sudumbreakar, N.; Schaffran, T.; Jenne, C.; Eriksson, J.; Winterhalter, M.; Fritz, J.; et al. Halogenated Dodecaborate Clusters as Agents to Trigger Release of Liposomal Contents. *ChemPlusChem* **2015**, *80*, 656–664. [[CrossRef](#)]

69. Gabel, D.; Awad, D.; Schaffran, T.; Radovan, D.; Dărăban, D.; Damian, L.; Winterhalter, M.; Karlsson, G.; Edwards, K. The Anionic Boron Cluster (B₁₂H₁₁SH)²⁻ as a Means To Trigger Release of Liposome Contents. *ChemMedChem* **2007**, *2*, 51–53. [[CrossRef](#)]
70. Lee, M.W.; Farha, O.K.; Hawthorne, M.F.; Hansch, C.H. Alkoxy derivatives of dodecaborate: Discrete nanomolecular ions with tunable pseudometallic properties. *Angew. Chem.* **2007**, *119*, 3078–3082. [[CrossRef](#)]
71. Joshi, M.; Ghanty, T.K. Hybrid Organic–Inorganic Functionalized Dodecaboranes and Their Potential Role in Lithium and Magnesium Ion Batteries. *J. Phys. Chem. C* **2018**, *122*, 27947–27954. [[CrossRef](#)]
72. Vishnoi, P.; Kaleeswaran, D.; Murugavel, R. 1,3,5-Triphenylbenzene: A versatile photoluminescent chemo-sensor platform and supramolecular building block. *RSC Adv.* **2018**, *8*, 17535–17550. [[CrossRef](#)]
73. Wu, Q.; Hook, A.; Wang, S. A Blue Luminescent Starburst Molecule and Its Orange Luminescent Trinuclear PdII Complex: 1,3,5-tris(7-azaindol-1-yl)benzene (tabH) and [Pd(tab)₂Cl₄]. *Angew. Chem. Int. Ed.* **2000**, *39*, 3933–3935. [[CrossRef](#)]
74. Dash, B.P.; Satapathy, R.; Bode, B.P.; Reidl, C.T.; Sawicki, J.W.; Mason, A.J.; Maguire, J.A.; Hosmane, N.S. “Click” Chemistry-Mediated Phenylene-Cored Carborane Dendrimers. *Organometallics* **2012**, *31*, 2931–2935. [[CrossRef](#)]
75. Dash, B.P.; Satapathy, R.; Gaillard, E.R.; Norton, K.M.; Maguire, J.A.; Chug, N.; Hosmane, N.S. Enhanced π -Conjugation and Emission via Icosahedral Carboranes: Synthetic and Spectroscopic Investigation. *Inorg. Chem.* **2011**, *50*, 5485–5493. [[CrossRef](#)] [[PubMed](#)]
76. Juárez-Pérez, E.J.; Viñas, C.; Teixidor, F.; Santillan, R.; Farfán, N.; Abreu, A.; Yépez, R.; Núñez, R. Polyanionic Aryl Ether Metallodendrimers Based on Cobaltabisdicarbollide Derivatives. Photoluminescent Properties. *Macromolecules* **2010**, *43*, 150–159. [[CrossRef](#)]
77. Zhou, H.; Ye, Q.; Xu, J. Polyhedral oligomeric silsesquioxane-based hybrid materials and their applications. *Mater. Chem. Front.* **2017**, *1*, 212–230. [[CrossRef](#)]
78. Laine, R.M.; Roll, M.F. Polyhedral Phenylsilsesquioxanes. *Macromolecules* **2011**, *44*, 1073–1109. [[CrossRef](#)]
79. Hartmann-Thompson, C. *Applications of Polyhedral Oligomeric Silsesquioxanes*; Springer: Midland, TX, USA, 2011.
80. Wang, M.; Chi, H.; KS, J.; Wang, F. Progress in the Synthesis of Bifunctionalized Polyhedral Oligomeric Silsesquioxane. *Polymers* **2019**, *11*, 2098. [[CrossRef](#)]
81. Maegawa, T.; Miyashita, O.; Irie, Y.; Imoto, H.; Naka, K. Synthesis and properties of polyimides containing hexaisobutyl-substituted T8 cages in their main chains. *RSC Adv.* **2016**, *6*, 31751–31757. [[CrossRef](#)]
82. Ro, H.W.; Soles, C.L. Silsesquioxanes in nanoscale patterning applications. *Mater. Today* **2011**, *14*, 20–33. [[CrossRef](#)]
83. Xia, S.; Yang, Y.; Zhu, W.; Lü, C. Quaternized polyhedral oligomeric silsesquioxanes stabilized Pd nanoparticles as efficient nanocatalysts for reduction reaction. *Colloids Surf., A* **2020**, *585*, 124110. [[CrossRef](#)]
84. Ghanbari, H.; Cousins, B.G.; Seifalian, A.M. A Nanocage for Nanomedicine: Polyhedral Oligomeric Silsesquioxane (POSS). *Macromol. Rapid Commun.* **2011**, *32*, 1032–1046. [[CrossRef](#)] [[PubMed](#)]
85. Li, Z.; Kong, J.; Wang, F.; He, C. Polyhedral oligomeric silsesquioxanes (POSSs): An important building block for organic optoelectronic materials. *J. Mater. Chem. C* **2017**, *5*, 5283–5298. [[CrossRef](#)]
86. Bahrami, M.; Furgal, J.C.; Hashemi, H.; Ehsani, M.; Jahani, Y.; Goodson, T.; Kieffer, J.; Laine, R.M. Synthesis and Characterization of Nanobuilding Blocks [o-RStyrPhSiO_{1.5}]_{10,12} (R = Me, MeO, NBoc, and CN). Unexpected Photophysical Properties Arising from Apparent Asymmetric Cage Functionalization as Supported by Modeling Studies. *J. Phys. Chem. C* **2015**, *119*, 15846–15858. [[CrossRef](#)]
87. Zhang, T.; Wang, J.; Zhou, M.; Ma, L.; Yin, G.; Chen, G.; Li, Q. Influence of polyhedral oligomeric silsesquioxanes (POSS) on blue light-emitting materials for OLED. *Tetrahedron* **2014**, *70*, 2478–2486. [[CrossRef](#)]
88. Sulaiman, S.; Bhaskar, A.; Zhang, J.; Guda, R.; Goodson, T.; Laine, R.M. Molecules with Perfect Cubic Symmetry as Nanobuilding Blocks for 3-D Assemblies. Elaboration of Octavinylsilsesquioxane. Unusual Luminescence Shifts May Indicate Extended Conjugation Involving the Silsesquioxane Core. *Chem. Mater.* **2008**, *20*, 5563–5573. [[CrossRef](#)]
89. Cheng, G.; Vautravers, N.R.; Morris, R.E.; Cole-Hamilton, D.J. Synthesis of functional cubes from octavinylsilsesquioxane (OVS). *Org. Biomol. Chem.* **2008**, *6*, 4662–4667. [[CrossRef](#)]
90. Itami, Y.; Marciniak, B.; Kubicki, M. Functionalization of Octavinylsilsesquioxane by Ruthenium-Catalyzed Silylative Coupling versus Cross-Metathesis. *Chem. Eur. J.* **2004**, *10*, 1239–1248. [[CrossRef](#)]

91. Anisimov, A.A.; Ol'shevskaya, V.A.; Novikov, R.A.; Korlyukov, A.A.; Buzin, M.I.; Shchegolikhina, O.I.; Kalinin, V.N.; Muzafarov, A.M. Polyfunctional carboranyl substituted octasilsesquioxane: Synthesis and characterization. *J. Organomet. Chem.* **2016**, *822*, 1–4. [[CrossRef](#)]
92. Farràs, P.; Teixidor, F.; Kivekäs, R.; Sillanpää, R.; Viñas, C.; Grüner, B.; Cisarova, I. Metallocarboranes as Building Blocks for Polyanionic Polyarmed Aryl-Ether Materials. *Inorg. Chem.* **2008**, *47*, 9497–9508. [[CrossRef](#)]
93. Sivaev, I.B.; Kulikova, N.Y.; Nizhnik, E.A.; Vichuzhanin, M.V.; Starikova, Z.A.; Semioshkin, A.A.; Bregadze, V.I. Practical synthesis of 1,4-dioxane derivative of the closo-dodecaborate anion and its ring opening with acetylenic alkoxides. *J. Organomet. Chem.* **2008**, *693*, 519–525. [[CrossRef](#)]
94. Teixidor, F.; Pedrajas, J.; Rojo, I.; Viñas, C.; Kivekäs, R.; Sillanpää, R.; Sivaev, I.; Bregadze, V.; Sjöberg, S. Chameleonic Capacity of $[3,3'-Co(1,2-C_2B_9H_{11})_2]^-$ in Coordination. Generation of the Highly Uncommon S(thioether)–Na Bond. *Organometallics* **2003**, *22*, 3414–3423. [[CrossRef](#)]
95. Chaari, M.; Gaztelumendi, N.; Cabrera-González, J.; Peixoto-Moledo, P.; Viñas, C.; Xochitiotzi-Flores, E.; Farfán, N.; Ben Salah, A.; Nogués, C.; Núñez, R. Fluorescent BODIPY-anionic boron cluster conjugates as potential agents for cell tracking. *Bioconjugate Chem.* **2018**, *29*, 1763–1773. [[CrossRef](#)] [[PubMed](#)]
96. Cabrera-González, J.; Muñoz Flores, B.M.; Viñas, C.; Chávez-Reyes, A.; Dias, H.V.R.; Jiménez Pérez, V.M.; Núñez, R. Organotin dyes bearing anionic boron clusters as cell-staining fluorescent probes. *Chem. Eur. J.* **2018**, *24*, 5601–5612.
97. Dash, B.P.; Satapathy, R.; Maguire, J.A.; Hosmane, N.S. Facile Synthetic Routes to Phenylene and Triazine Core Based Dendritic Cobaltabisdicarbollides. *Organometallics* **2010**, *29*, 5230–5235. [[CrossRef](#)]
98. Semioshkin, A.A.; Las'kova, Y.N.; Zhidkova, O.B.; Bregadze, V.I. Synthesis of new building blocks based on the closo-dodecaborate anion. *Russ. Chem. Bull.* **2008**, *57*, 1996–1998. [[CrossRef](#)]
99. Semioshkin, A.; Tsaryova, O.; Zhidkova, O.; Bregadze, V.; Wöhrle, D. Reactions of oxonium derivatives of $(B_{12}H_{12})^{2-}$ with phenoles, and synthesis and photochemical properties of a phthalocyanine containing four $(B_{12}H_{12})^{2-}$ groups. *J. Porphyr. Phthalocyanines* **2006**, *10*, 1293–1300. [[CrossRef](#)]
100. Prikaznov, A.V.; Las'kova, Y.N.; Semioshkin, A.A.; Sivaev, I.B.; Kisin, A.V.; Bregadze, V.I. Synthesis of boron-containing tyrosine derivatives based on the closo-decaborate and closo-dodecaborate anions. *Russ. Chem. Bull.* **2011**, *60*, 2550–2554. [[CrossRef](#)]
101. Grubbs, R.H.; O'Leary, D.J. *Handbook of Metathesis: Applications in Organic Synthesis*; John Wiley & Sons: Weinheim, Germany, 2015.
102. Cioran, A.M.; Teixidor, F.; Viñas, C. The effect of a paramagnetic metal ion within a molecule: Comparison of the structurally identical paramagnetic $[3,3-Fe(1,2-C_2B_9H_{11})_2]^-$ with the diamagnetic $[3,3-Co(1,2-C_2B_9H_{11})_2]^-$ sandwich complexes. *Dalton Trans.* **2015**, *44*, 2809–2818. [[CrossRef](#)]
103. Kukhta, N.A.; Volyniuk, D.; Peciulyte, L.; Ostrauskaite, J.; Juska, G.; Grazulevicius, J.V. Structure–property relationships of star-shaped blue-emitting charge-transporting 1,3,5-triphenylbenzene derivatives. *Dyes Pigment.* **2015**, *117*, 122–132. [[CrossRef](#)]
104. Khotina, I.A.; Lepnev, L.S.; Burenkova, N.S.; Valetsky, P.M.; Vitukhnovsky, A.G. Phenylene dendrimers and novel hyperbranched polyphenylenes as light emissive materials for blue OLEDs. *J. Lumin.* **2004**, *110*, 232–238. [[CrossRef](#)]
105. Núñez, R.; Juárez-Pérez, E.J.; Teixidor, F.; Santillan, R.; Farfán, N.; Abreu, A.; Yépez, R.; Viñas, C. Decorating Poly(alkyl aryl-ether) Dendrimers with Metallocarboranes. *Inorg. Chem.* **2010**, *49*, 9993–10000. [[CrossRef](#)] [[PubMed](#)]
106. Rojo, I.; Teixidor, F.; Viñas, C.; Kivekäs, R.; Sillanpää, R. Relevance of the Electronegativity of Boron in η^5 -Coordinating Ligands: Regioselective Monoalkylation and Monoarylation in Cobaltabisdicarbollide $[3,3'-Co(1,2-C_2B_9H_{11})_2]^-$ Clusters. *Chem. Eur. J.* **2003**, *9*, 4311–4323. [[CrossRef](#)] [[PubMed](#)]
107. André, P.; Cheng, G.; Ruseckas, A.; van Mourik, T.; Früchtl, H.; Crayston, J.A.; Morris, R.E.; Cole-Hamilton, D.; Samuel, I.D.W. Hybrid Dendritic Molecules with Confined Chromophore Architecture to Tune Fluorescence Efficiency. *J. Phys. Chem. B* **2008**, *112*, 16382–16392. [[CrossRef](#)] [[PubMed](#)]
108. Furgal, J.C.; Jung, J.H.; Goodson, T.; Laine, R.M. Analyzing Structure–Photophysical Property Relationships for Isolated T8, T10, and T12 Stilbenevinylsilsesquioxanes. *J. Am. Chem. Soc.* **2013**, *135*, 12259–12269. [[CrossRef](#)]

109. Niemczyk, A.; Dziubek, K.; Sacher-Majewska, B.; Czaja, K.; Czech-Polak, J.; Oliwa, R.; Lenza, J.; Szolyga, M. Thermal Stability and Flame Retardancy of Polypropylene Composites Containing Siloxane-Silsesquioxane Resins. *Polymers* **2018**, *10*, 1019. [[CrossRef](#)] [[PubMed](#)]
110. Cordes, D.B.; Lickiss, P.D.; Rataboul, F. Recent Developments in the Chemistry of Cubic Polyhedral Oligosilsesquioxanes. *Chem. Rev.* **2010**, *110*, 2081–2173. [[CrossRef](#)]
111. Yang, D.; Zhang, W.; Yao, R.; Jiang, B. Thermal stability enhancement mechanism of poly(dimethylsiloxane) composite by incorporating octavinyl polyhedral oligomeric silsesquioxanes. *Polym. Degrad. Stab.* **2013**, *98*, 109–114. [[CrossRef](#)]
112. Lakowicz, J.R. *Principles of Fluorescence Spectroscopy*; Springer US: Baltimore, MD, USA, 2007.
113. Brouwer, A.M. Standards for photoluminescence quantum yield measurements in solution (IUPAC Technical Report). *Pure Appl. Chem.* **2011**, *83*, 2213–2228. [[CrossRef](#)]

Sample Availability: Samples of the compounds are available from the authors.



© 2020 by the authors. Licensee MDPI, Basel, Switzerland. This article is an open access article distributed under the terms and conditions of the Creative Commons Attribution (CC BY) license (<http://creativecommons.org/licenses/by/4.0/>).